THE ASTROPHYSICAL JOURNAL, 377:L41–L44, 1991 August 10


# FIRST RESULTS FROM THE GODDARD HIGH-RESOLUTION SPECTROGRAPH: A DEMONSTRATION OF SPECTRAL RESOLUTION AND EXPERIMENTS WITH DECONVOLUTION

GLENN M. WAHLGREN,[1,6] DAVID S. LECKRONE,[2,3,6] STEVEN N. SHORE,[1,4,6] DON J. LINDLER,[5,6]
RONALD L. GILLILAND,[7] AND DENNIS C. EBBETS[3,8]
*Received 1991 March 29; accepted 1991 April 19*

## ABSTRACT

High-quality spectra of the sharp-lined star $\chi$ Lupi were obtained with the Goddard High Resolution Spectrograph (GHRS). We display spectra for the various resolving powers achievable with the echelle and G160M gratings. The effect of spherical aberration upon the spectral resolution is found to be negligible when using the small science aperture. The resolution of the large science aperture spectra is degraded by less than a factor of 2. Our efforts with spectral deconvolution using several techniques show that it is possible to regain much of the spectral resolution lost in the large science aperture if high signal-to-noise spectra are obtained.

*Subject headings:* instruments — numerical methods — stars: individual ($\chi$ Lupi) — ultraviolet: spectra

## 1. INTRODUCTION

Observations of the extremely sharp-lined chemically peculiar star $\chi$ Lupi (HD 141556) were made with the Goddard High Resolution Spectrograph (GHRS) on the *Hubble Space Telescope* (*HST*) as part of the early Science Assessment Observation program. The choice of this target, coupled with the design of the observing program, provides data that aid in characterizing the performance of the GHRS, with regard to dense absorption-line spectra, while addressing problems in stellar photospheres, elemental abundances in chemically peculiar stars, and atomic physics.

The prelaunch characteristics and proposed operation of the GHRS have been described by Duncan & Ebbets (1990). While the internal performance of the GHRS can still be described by much of the prelaunch analysis, its actual performance has been affected by spherical aberration discovered in the *HST* primary telescope mirror. Burrows et al. (1991) have outlined the current understanding of spherical aberration as it pertains to *HST* imaging and spacecraft operations. The effect upon spectral observations is evident from the results presented here and by others in this volume.

The result of spherical aberration is to deliver to the GHRS a point spread function (psf) that contains only about 16% of the light concentrated within a 0.″1 radius, as opposed to the design specification of 70%. This aberrated psf manifests itself in different ways for the two GHRS science apertures. The large science aperture (LSA) is a square that measures 2″ on a side and is large enough to include 70% of the light. Thus the LSA psf degrades spectral resolution while maintaining the throughput to within a factor of 2. The small science aperture (SSA), however, is only 0.″25 on a side. It has the effect of rejecting the wings of the psf while retaining the core characteristics. The SSA underfills the height of a science diode, and its spectrum is therefore sampled differently than that of the LSA. The SSA data are not noticeably degraded in spectral resolution, but the performance suffers from a throughput loss requiring an increase in exposure time to produce a given signal-to-noise (S/N) level. At the wavelength of the observations presented here the SSA exposure time was increased by a factor of 5.5 to reproduce the S/N level of prelaunch expectations.

## 2. OBSERVATIONS AND DATA REDUCTION

$\chi$ Lupi (B9.5p, $V = 3.95$) is a bright, nonmagnetic chemically peculiar star with an extremely low rotational velocity ($v \sin i < 1.2$ km s$^{-1}$). Its ultraviolet spectrum is rich in absorption lines, predominantly of doubly ionized atomic species. These qualities make it an excellent target for displaying the spectral resolving power of the GHRS. The observing program was designed to provide data in several observing modes, or aperture/grating combinations, in order to address the question of the instrument's resolving power in light of spherical aberration and to allow for experiments in spectral deconvolution.

The program was executed on 1991 February 11. For each observation we used the standard FP-SPLIT option, producing four subexposures at slightly different carousel settings. Each subexposure was quarter-stepped (quarter-diode sampling at a fixed carousel position), producing four bins of science data with 500 samples per bin. For the SSA/Ech-B observation it was necessary to divide the total exposure time into three exposures. The FP-SPLIT option would then produce a matrix of 12 subexposures; three at each carousel setting. As a result of an observatory anomaly the subexposures of the first FP-SPLIT carousel position for the SSA/Ech-B observation along with one of the two ensuing wavelength calibrations were lost. Table 1 lists the journal of observations.

The exposure times were determined to provide high photometric quality data with an approximate S/N level of 100 in the

[1] Astronomy Programs, Computer Sciences Corporation, GHRS Science Team.
[2] Laboratory for Astronomy and Solar Physics, NASA/Goddard Space Flight Center.
[3] Goddard High Resolution Spectrograph Investigation Definition Team.
[4] DEMIRM, Obs. de Meudon.
[5] Advanced Computer Concepts, Inc.
[6] Postal address: Code 681, Goddard Space Flight Center, Greenbelt, MD 20771.
[7] Postal address: Space Telescope Science Institute, 3700 San Martin Drive, Baltimore, MD 21218.
[8] Postal address: Ball Aerospace Systems Group, GHRS Project/JWF-3, Ball Aerospace, P.O. Box 1062, Boulder, CO 08306-1062.

TABLE 1

PARAMETERS OF THE $\chi$ LUPI OBSERVATIONS

| OBSERVATION ID | DATE[a] (JD −2,440,000) | APERTURE/GRATING | SPECTRAL COVERAGE (Å) | NUMBER OF SUBEXPOSURES[b] | EXPOSURE TIME/[c] SUBEXPOSURE (s) | AVERAGE COUNT RATE[d] | |
|---|---|---|---|---|---|---|---|
| | | | | | | Background | Stellar |
| Z0G70106 ..... | 8299.365 | LSA/G160M | 1924.7–1959.3 | 4 | 80.784 | 0.269 | 104.689 |
| Z0G70108 ..... | 8299.378 | LSA/Ech-B[e] | 1936.7–1947.1 | 4 | 215.424 | 5.856 | 54.993 |
| Z0G7010G..... | 8299.450 | SSA/G160M | 1924.7–1959.3 | 4 | 242.352 | 0.072 | 28.568 |
| Z0G7010J ..... | 8299.526 | SSA/Ech-B[e] | 1936.8–1947.0 | 9 | 269.280 | 1.315 | 15.178 |

[a] Date corresponds to the Unique Data Log readout start time, following the last subexposure.

[b] Number of subexposures corresponds to the number of FP-SPLIT subexposures. The SSA/Ech-B observation obtained data at only the last three carousel settings.

[c] Exposure time for all 6 data bins, 4 science and 2 background. Exposure time for science data is 0.94 times the listed value, the remainder being spent on background data collection. Step patterns of 7 and 5 were used for the Ech-B and G160M gratings, respectively.

[d] Count rate, in counts/s/sample/subexposure. Note that the background in the first-order grating is a small fraction of the on-order data.

[e] Order 29 within Echelle-B.

stellar continuum for each data sample. The exposure times were further constrained so that no subexposure would last longer than approximately 5 minutes. Analysis of GHRS Science Verification (SV) data has shown that the spectrum drifts on the diode array due to the changing thermal and magnetic environments during a single orbit. The total drift rate has been measured to be as large as 0.06 diodes minute$^{-1}$, with an amplitude of $\pm 0.5$ diode, and it is capable of degrading the spectral resolution on long exposures. Limiting an individual FP-SPLIT subexposure to less than 5 minutes alleviates this problem.

The imaging capabilities of the GHRS were used to provide information on the centering of the star within the apertures. Position of the stellar image with respect to the aperture center will affect the wavelength scale, total number of counts recorded, and the shape of the line spread function (lsf). Target acquisition procedures placed the star within 0".1 of the LSA center. Count rates with the A2 mirror were typically 5550 counts per integration period (200 ms) during the target acquisition phase. This count rate is approximately one-third of the prelaunch sensitivity for this mirror and also reflects the effect of spherical aberration. To center the target in the SSA the stellar image was first centered in the LSA with a PEAKUP procedure, followed by an offset slew to the SSA calibrated during SV testing.

Image jitter induced by the day-to-night orbital transition's effect upon the solar array panels can be as large as 0".2, which is nearly the size of the SSA. Our data did show the signature of such jitter. With the exception of the LSA/Ech-B observation, the remaining spectral observations were scheduled concurrently with Earth shadow exit. The LSA/G160M data displayed no noticeable deviation in the count rate among the subexposures. For both SSA observations the shadow exit appears to have occurred near the start of a subexposure. The count rates in the SSA/G160M data were reduced by 10% from the preshadow exit values. The SSA/Ech-B data were reduced by approximately 6%. In both cases the reduction in count rate affected spectra being taken for no more than 10 minutes from shadow exit, after which the count rates returned to preshadow-exit levels.

The data were reduced with the CALHRS software package (Lindler 1989). Subexposures were reduced individually, combining four bins of spectral data. The two background data bins were similarly reduced, averaged, and fitted with a third-order polynomial prior to being subtracted from the spectral data. The FP-SPLIT subexposures were cross-correlated with the first subexposure to determine the offsets. The subexposures were registered to the nearest sample position and co-added. The wavelength calibration employed standard platinum lamp observations scheduled immediately prior to the stellar spectrum. The standard wavelength position was not at the wavelength of our observations but is adequate for determining the wavelength scale to better than one diode.

## 3. SPECTRAL RESOLUTION

The ultimate benefit of the GHRS over previous space-based observatories lies in its ability to achieve high photometric accuracy at high spectral resolution. Properly exposed *IUE* high-dispersion spectra typically have a S/N level $< 20$ at a resolving power of $R = 12{,}000$. It is possible to increase the S/N ratio of *IUE* data for absorption spectra through a process of co-addition of multiple exposures (Leckrone & Adelman 1989). *Copernicus* satellite spectra were of a higher spectral resolution, up to $R = 30{,}000$, but high S/N was typically achieved only on bright stars over a limited wavelength range (Rogerson et al. 1973).

To illustrate the spectral resolution capabilities of the GHRS we display in Figure 1 a 2 Å interval of the $\chi$ Lupi spectrum obtained with *IUE* and the GHRS. The *IUE* spectrum is a single, small aperture, high-dispersion observation (SWP 4688H) having an exposure time of 255 s. Below it, in order of increasing resolving power, are the four GHRS modes from this program. The spectra have been normalized to their respective continuum levels by a procedure which makes use of synthesized spectra. For the SSA/Ech-B spectrum the continuum was estimated to lie within a fraction of 1% of the observed data.

All of the GHRS spectra have a higher S/N and spectral resolution than the *IUE* spectrum. At $\lambda 1940$ the instrumental resolution of the G160M and Ech-B modes are $R = 28{,}000$ and 87,000, respectively. These resolving powers are realized in the SSA data. Comparison of LSA and SSA spectra obtained with the same grating shows the effect of spherical aberration. From our work with these spectra, it appears that the effective resolving power in the LSA is decreased by less than a factor of 2.

## 4. SPECTRAL DECONVOLUTION

The basic problem of deconvolution for a spectrum is to determine, given the optical transform of the telescope plus spectrograph $\Pi(x \mid y)$, the form of the input spectrum $S(y)$ from

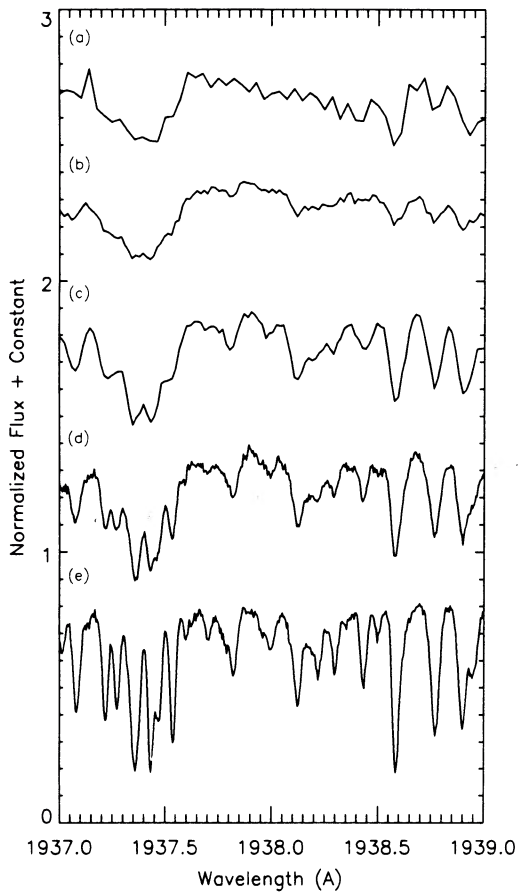


FIG. 1.—Spectral resolution capabilities of the GHRS. An *IUE* spectrum (*a*) is compared with GHRS spectra taken in modes (*b*) LSA/G160M, (*c*) SSA/G160M, (*d*) LSA/Ech-B, and (*e*) SSA/Ech-B. The normalized spectra have been arbitrarily displaced for plotting purposes. The S/N in the continuum of the GHRS spectra is between 90 and 100, as compared to <20 for the *IUE* spectrum. The effect of spherical aberration on LSA spectra can be seen by comparing spectra (*b*) with (*c*), and (*d*) with (*e*).

the observed spectrum $D(x)$, via solution of the integral equation:

$$D(x) = \int \Pi(x \mid y) S(y) dy \, . \quad (1)$$

In our case, the quantity $\Pi(x \mid y)$, the probability that result $x$ is obtained from input $y$, is a continuous redistribution operator known as the line spread function. We have explored several techniques aimed at solving the integral equation, given a model lsf, including a Richardson-Lucy (R-L) algorithm (Richardson 1972; Lucy 1974), a constrained block-iterative approach (Heap & Lindler 1987), a nonlinear constrained iteration (Jansson 1984), and Fourier-Wiener filtering (Press et al. 1986).

In the context of the GHRS, the recovery of resolution from LSA observations requires a model lsf at the wavelength of the observation. We have constructed such a model lsf using a stellar image taken with the Faint Object Camera (FOC) through the F210M medium-band filter. The FOC image was taken through a broad enough bandpass that some of the intrinsic structure present in the large aperture lsf is washed out. The FOC aperture lies nearly opposite the GHRS in the telescope focal plane at roughly the same axial distance. A

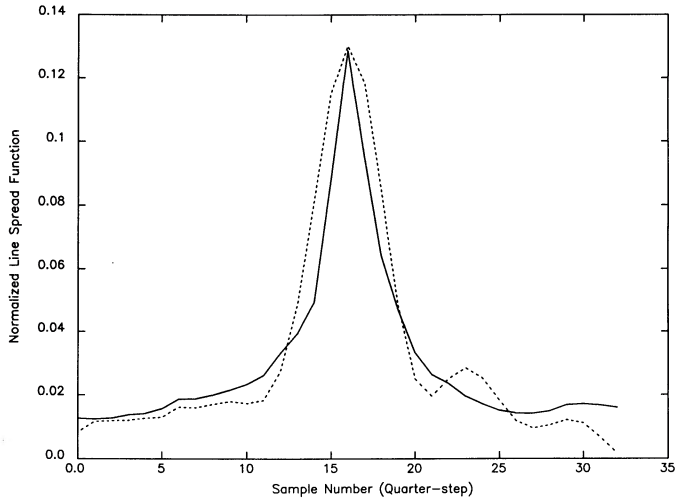


FIG. 2.—Comparison of lsf models for the G160M grating. *Solid line:* model lsf created from an FOC stellar image. *Dashed line:* lsf derived by a constrained least-squares approach relating the LSA spectrum to that of the SSA. The GHRS-derived lsf is broader in the core and shows a bump on one side. Using the echelle data the derived lsf is more symmetric, does not display a bump, and is broader in the core than the FOC model lsf.

constant background level was subtracted, and the lsf was formed by summing over the height of the LSA, equivalent to a 2″ line centered on the image peak. The G160M lsf wings were then clipped at ±1″ from peak center and binned to the sample size of the observed LSA spectrum. The deconvolution algorithm works in sample units rather than on an absolute wavelength scale. The echelle lsf was similarly constructed but resampled to the resolution of the echelle optics. The model lsf for the G160M grating is presented in Figure 2.

The result of deconvolving the LSA data with the normal-

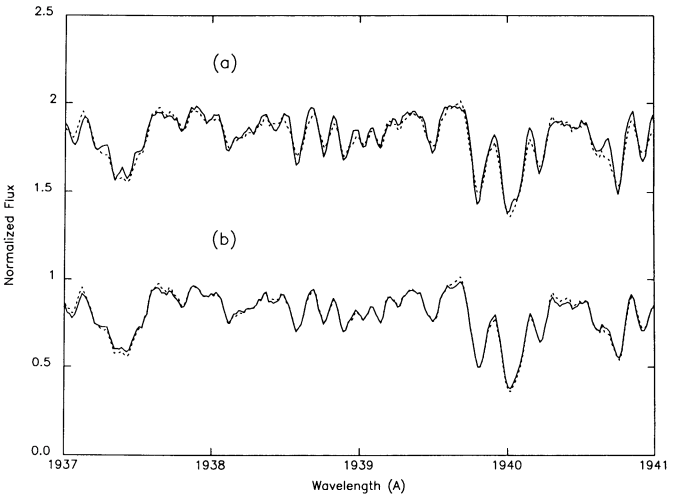


FIG. 3.—Deconvolution tests with the first-order (G160M) spectrum. (*a*) Comparison of observed SSA "truth" spectrum (*solid*) with the LSA spectrum deconvolved with the FOC lsf (*dash*) by a Richardson-Lucy algorithm. Deconvolved spectrum has been renormalized by a constant factor to account for the relative difference in the continuum level at the two resolutions, before and after deconvolution. (*b*) Comparison of deconvolutions using the two lsf's of Fig. 2, FOC model (*dashed line*) and GHRS-derived (*solid line*). The results are strikingly similar, showing the relative insensitivity of the deconvolution process to these lsf's.

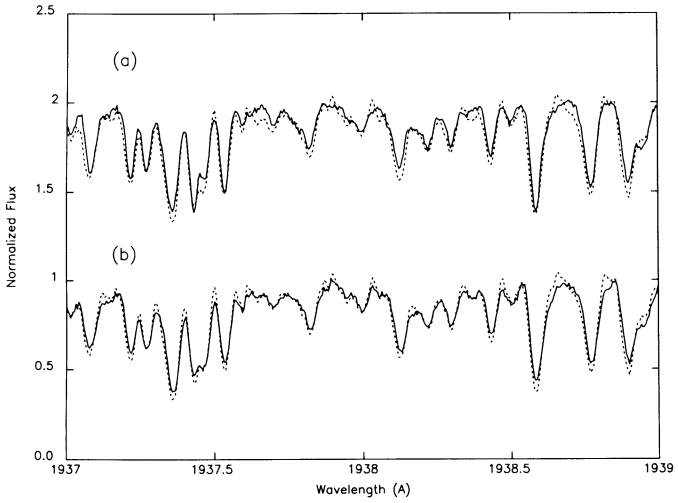


FIG. 4.—Deconvolution tests with the echelle (Ech-B) spectrum. Display is as in Fig. 3. Several of the largest differences in the upper comparison are amplifications, by the deconvolution process, of real differences between the spectra.

ized model lsf is presented in Figures 3 and 4 for the G160M and echelle, respectively, compared against the appropriate SSA, or "truth," spectrum. The fits are quite encouraging, but deviations at the 5% level are present. The major discrepancies between deconvolved LSA and observed SSA echelle spectra appear as absorption-like features in the LSA spectrum that have been amplified by the deconvolution process. Comparison of the actual LSA and SSA spectra shows artifacts that are larger than the noise level. Such artifacts in an essentially noiseless spectrum place a real limit on the veracity of features in the deconvolved LSA spectrum, regardless of the line strength.

As a test of the model lsf, the inverse problem of deriving a relative lsf directly from the LSA and SSA data was undertaken. Conceptually, one solves for the lsf that produces the best approximation to the observed LSA spectrum when convolved with the observed SSA spectrum. We adopted a nonlinear constrained least-squares technique. For the G160M grating the result is an asymmetric lsf having a broader core and a distinct bump of relative amplitude 20% on one side. A similarly produced echelle lsf does not show such an asymmetry. These lsf's are consistent with this data set, but must also reflect the relative differences between apertures for the light path, fixed pattern noise, and photon noise. The sensitivity of the deconvolution technique to the lsf is presented in the lower portions of Figures 3 and 4. The two lsf's, considered to represent reasonable bounds for a lsf, produce quite similar results. Not shown is the comparison of results between the different algorithms. These differences were found to be smaller than the differences resulting from the two lsf's in Figure 2.

## 5. DISCUSSION

With proper program design and data reduction procedures the GHRS produces ultraviolet spectra of unprecidented S/N and resolution. The resolving power in the SSA spectra is consistent with prelaunch expectations, while that of the LSA is degraded by less than a factor of 2 due to spherical aberration. Some recovery of resolution is possible for LSA data using deconvolution techniques. Noise in the data, uncertainty in the lsf, and the differences in sampling the science diode array by the two apertures are, however, limiting factors in the application of deconvolution to GHRS data.

Differences between the observed SSA and deconvolved LSA spectra exist at the level of 2–3 $\sigma$ of the continuum. Observed LSA spectra contain structure which is not present in the SSA spectra, and which is amplified by the deconvolution process. We also find deconvolved spectra to be less sensitive to the specific algorithm than to uncertainties in the model lsf. We conclude from the tests that the SSA should be used when performing a fine analysis of weak features or very accurate measurements of relative line strengths.

This work was supported by NASA Guaranteed Time Observer funding to the GHRS science team.

## REFERENCES

Burrows, C. J., Holtzman, J. A., Faber, S. M., Bely, P. Y., Hasan, H., Lynds, C. R., & Schroeder, D. 1991, ApJ, 369, L21
Duncan, D. K., & Ebbets, D. 1990, Goddard High Resolution Spectrograph Instrument Handbook, Version 2 (Baltimore: STScI)
Heap, S. R., & Lindler, D. J. 1987, A&A, 815, L10
Jansson, P. A. 1984, Deconvolution: With Applications in Spectroscopy (New York: Academic)
Leckrone, D. S., & Adelman, S. J. 1989, ApJS, 71, 387
Lindler, D. J. 1989, Goddard High Resolution Spectrograph: Data Management and Analysis Software Operator/User Manual (Potomac: Advanced Computer Concepts, Inc.)
Lucy, L. B. 1974, AJ, 79, 745
Press, W. H., Flannery, B. P., Teukolsky, S. A., & Vetterling, W. T. 1986, Numerical Recipes: The Art of Scientific Computing (Cambridge: Cambridge University Press)
Richardson, W. H. 1972, J. Opt. Soc. Am., 62, 55
Rogerson, J. B., Spitzer, L., Drake, J. F., Dressler, K., Jenkins, E. B., Morton, D. C., & York, D. G. 1973, ApJ, 181, L97